Formic Acid Photoreforming for Hydrogen Production on Shape-Controlled Anatase TiO₂ Nanoparticles: assessment of the role of Fluorides, {101}/{001} Surfaces Ratio and Platinization

Francesco Pellegrino[a*], Fabrizio Sordello[a], Lorenzo Mino[a], Claudio Minero[a], Vasile-Dan Hodoroaba[b], Gianmario Martra[a], Valter Maurino[a*]

a) Chemistry Department and NIS (Nanostructured Interfaces and Surfaces) inter-dipartimental centre, University of Torino, Via P. Giuria 7, Torino, 10125, Italy
b) Federal Institute for Materials Research and Testing (BAM), 12205 Berlin, Germany

*Corresponding authors: francesco.pellegrino@unito.it; Tel: +39 011 6705297;

valter.maurino@unito.it; Tel: +39 011 6705218;

1. Synthesis and Characterization of the materials (see also ref.[1])

n-sh. The synthesis of TiO₂ nano-sheets was carried out using a solvothermal method.[2] In a typical synthesis, an precise volume of Ti(OBu)₄ (Aldrich reagent grade 97%) was poured into a Teflon lined stainless steel reactor and the desired volume of concentrated hydrofluoric acid (Aldrich reagent grade 47%) was added dropwise under stirring. The reactor was sealed and kept under stirring at 523 K for 24 hours. The resulting paste was centrifuged and washed several times with acetone to remove the residual organics and then with water (Milli-Q). The final aqueous suspension was freeze-dried obtaining a bluish powder. The blue colour is due to the F⁻ doping of the anatase. This material exposes nearly 20% of the surface {101}.

n-sh_NaOH. Surface's fluorides were removed washing the as-synthesized material (n-sh) with 0.1 M NaOH solution (2 hours under stirring at room temperature)[3]. After NaOH treatment, the NPs were washed with HNO₃ 0.1 M to remove Na⁺ ions from the surface and finally again with ultrapure water (MilliQ, Millipore). This material exposes nearly 20% of the surface {101}.

n-sh_873K. For a complete removal of the fluorides from the nanoparticles, the as-synthesized material (n-sh) was heated at 873 K for 1 hour in air (ramp of near 6 K min⁻¹). The resulting powder is white. This material exposes nearly 40% of the surface {101}, due to the calcination treatment that induces a coalescence of the nanoparticles along the c-axis. The thermal treatment at 873 K induces also a (1x4) reconstruction of the {001} surface (see ref.[1] for further details).

bipy_873K. The material named bipy_873K was obtained by forcing the hydrolysis of a 40 mM aqueous solution of Ti(TeoaH)₂ complex (TeoaH = triethanolamine; initial pH 10), carried out by hydrothermal treatment at 453 K for 90 hours in autoclave. The material was then heated at 873 K for 1 hour in air atmosphere (ramp of near 6 K min⁻¹). Further details on the preparation and characterization of these NPs, which show a bipyramidal shape, can be found in our previous publication[4]. This material exposes nearly 90% of the surface {101}.

2. Fluorides Quantitation

Fluorides are added as shape controllers. They selectively adsorb at (001) surface increasing its quantity as described in more papers, e.g.[5]. In a previous work,[1] we checked the amounts of fluorides present in the nanosheets together with a full description of the syntheses methods. In that work the presence of fluorides in the nanoparticles was quantified by ion chromatography and TOF-SIMS (Time-of-Flight Secondary Ion Mass Spectrometry) analysis. The results are reported in Table S1.

While the NaOH-treated sample has a significantly reduced fluoride content compared with the pristine material (25-55%) – coherent with the loss of surface fluorides – the calcined nanosheets have lost > 95% of the fluorides originally present, confirming that also bulk fluorides can be removed by means of high temperature treatment.

Table S1. Fluoride content found in the TiO$_2$ nanosheets synthesized and studied in the present work.

Name	IC (mg F$^-$/g TiO$_2$)	TOF-SIMS I$_{F^-}$/ITiO$_2^-$ (a.u.)
n-sh	16.1 ± 1.2	73 ± 6
n-sh_NaOH	7.0 ± 0.8	54 ± 4
n-sh_873K	< 0.4	3.6 ± 0.4[a]

[a]This concentration level was found even in the Si (100) blank substrate used for analysis, demonstrating that this level of F$^-$ represents the background contamination present at the TOF-SIMS instrument used.

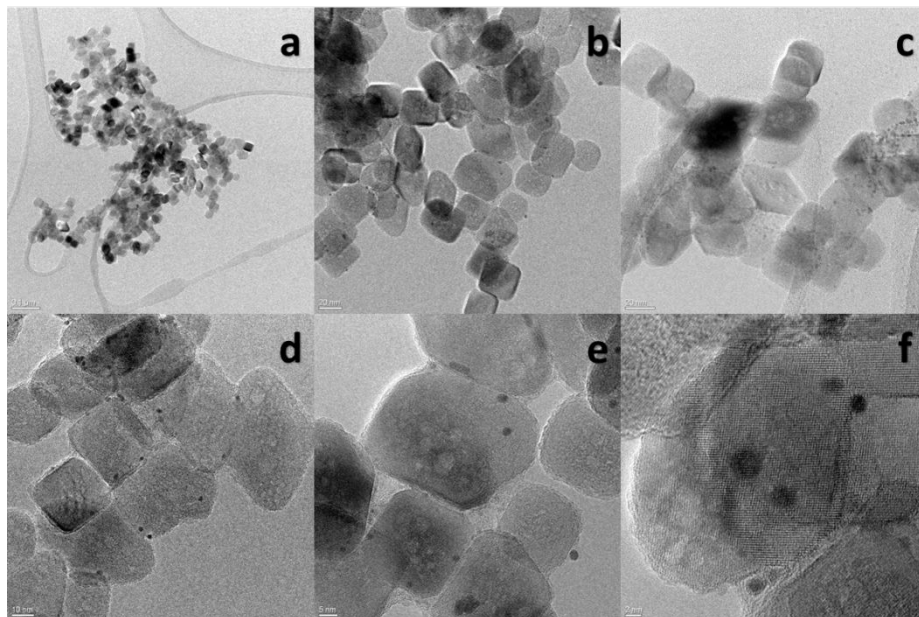## 3. Supplementary TEM Micrographs and Pt NPs distribution analysis

✓ **bipy_873K**

Figure S1. TEM of the material *bipy* after the Pt photodeposition. Scale bars: a) 100 nm; b) 20 nm; c) 20 nm; d) 10 nm; e) 5 nm; f) 2 nm
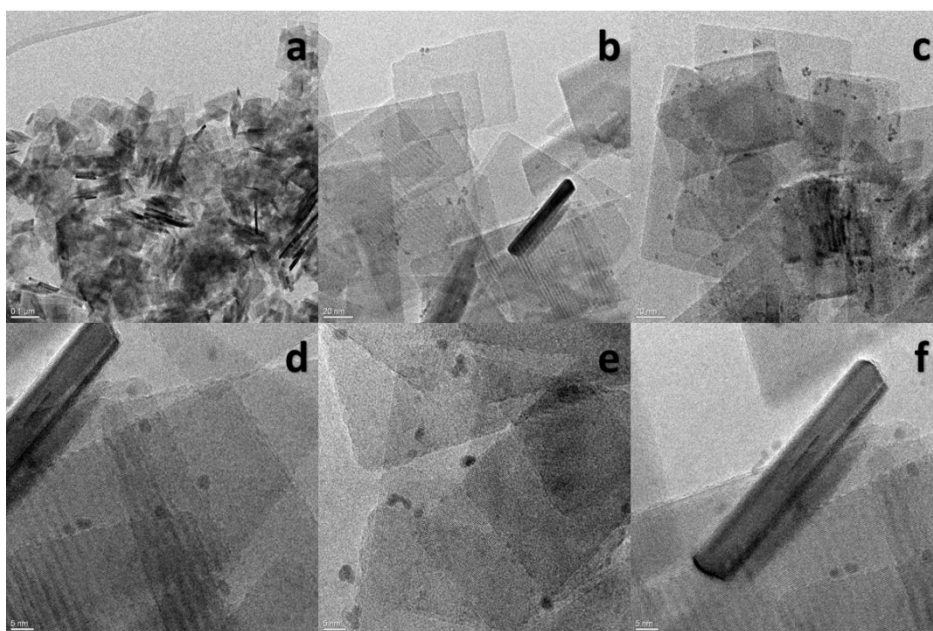
✓ **n-sh**

Figure S2. TEM of the material *n-sh* after the Pt photodeposition. Scale bars: a) 100 nm; b) 20 nm; c) 20 nm; d) 5 nm; e) 5 nm; f) 5 nm
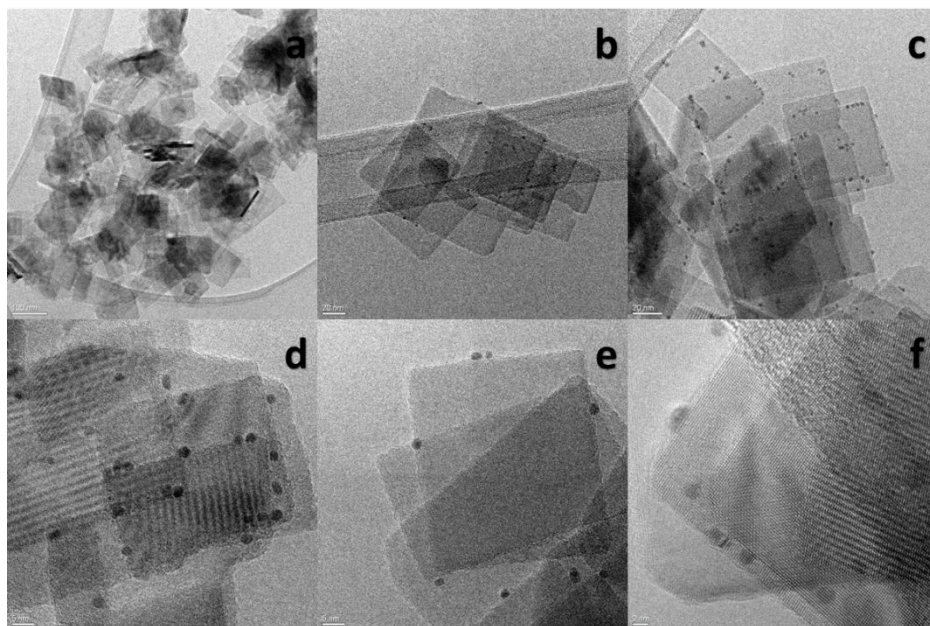
✓ **n-sh_NaOH**

Figure S3. TEM of the material *n-sh_NaOH* after the Pt photodeposition. Scale bars: a) 100 nm; b) 20 nm; c) 20 nm; d) 5 nm; e) 5 nm; f) 2 nm
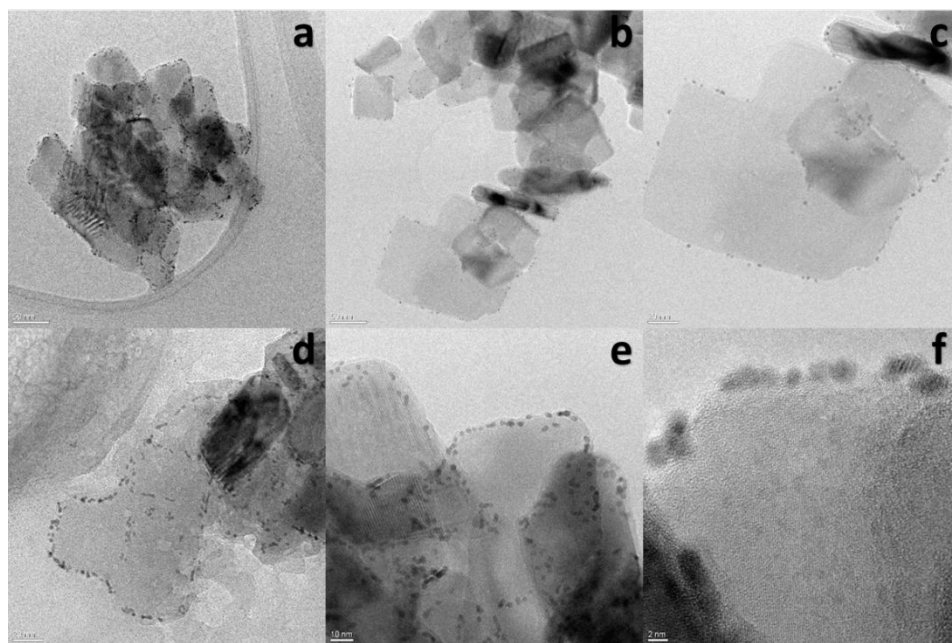
✓ **n-sh_873K**

Figure S4. TEM of the material *n-sh_873K* after the Pt photodeposition. Scale bars: a) 50 nm; b) 50 nm; c) 20 nm; d) 20 nm; e) 10 nm; f) 2 nm

Table S2. Pt NPs dimensional analysis and density distribution on TiO$_2$ nanoparticles

Material Name	Pt Size, nm	Density, Pt NPs m^{-2}
n-sh	2.2 ± 0.4	4x10^{-14}
n-sh_NaOH	2.3 ± 0.3	4x10^{-14}
n-sh_873K	2.3 ± 0.4	6x10^{-14}
bipy_873K	2.3 ± 0.4	1x10^{-14}

In Table S2 and Figure S5 we reported the dimensional analysis of the photodeposited Pt NPs from TEM micrographs together with the density of Pt nanoparticles on the {101} TiO$_2$ surface. The size of the Pt NPs is nearly the same for all the four materials considered, so the differences on the photocatalytic activity cannot be ascribed to the differences in the Pt NPs size. As said in the main text, the density of Pt nanoparticles is higher in the case of the nanosheets due to the lower amount of {101} TiO$_2$ surface compared to the bipyramids (at the same % weight of Pt). This confirms the conclusions drawn about the change in the {101} TiO$_2$ surface activity in the presence of Pt (Figure 4 of the main text). However, it must be taken into account that the distribution of the Pt NPs reported in Table S2 is not perfectly homogeneous, and it is hard to estimate their uncertainty. Therefore, Pt NPs density could be slightly different in the whole sample compared with the portions examined with TEM. In general, nanosheets have larger Pt NPs density compared with bipyramidal TiO$_2$ NPs.
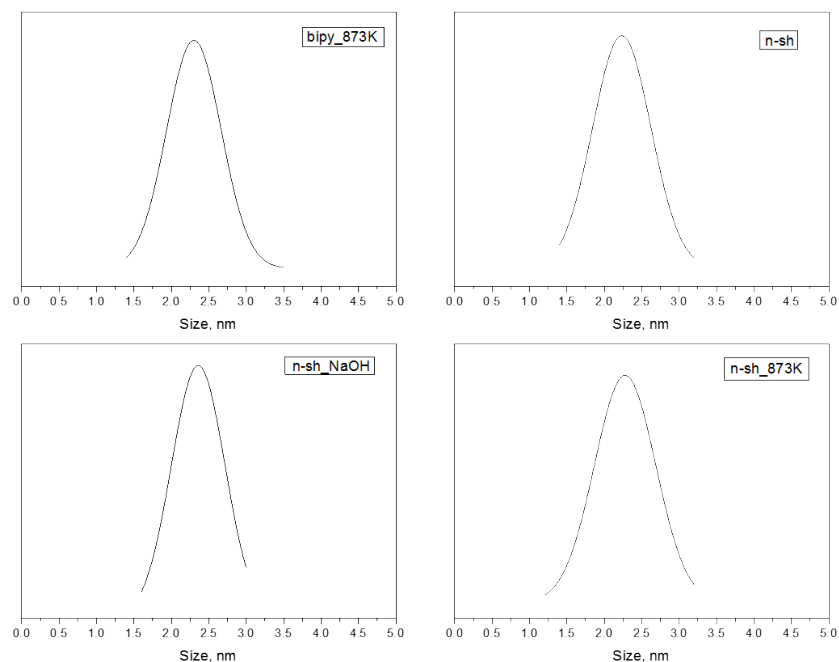

Figure S5. Normal distribution of the Pt NPs size carried out starting from the TEM analysis.

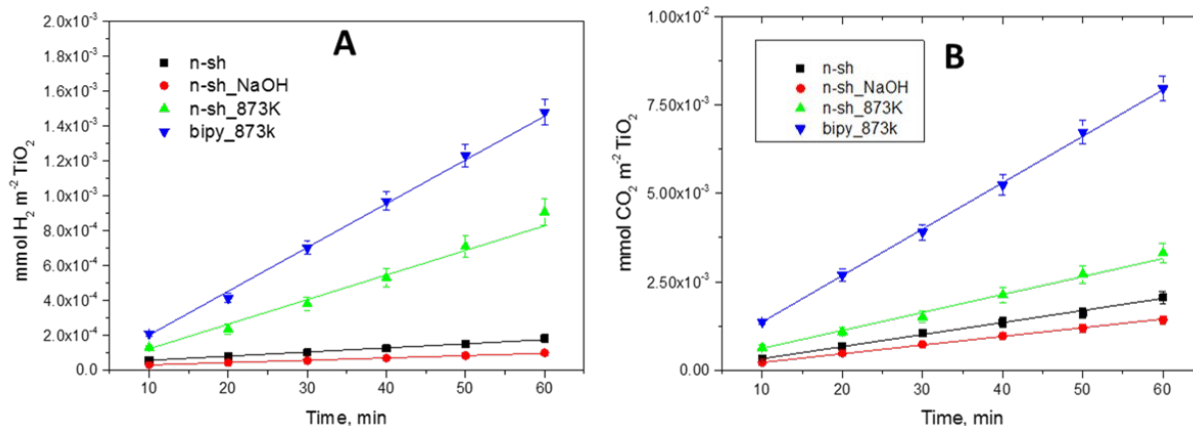## 4. Photocatalytic H_2 and CO_2 production

Figure S6. Photocatalytic H_2 (A) and CO_2 (B) production curves obtained at pH 3.5 for the studied materials without Pt as co-catalyst. The results are normalized for the SSA of the TiO_2 material used.

Hydrogen and CO_2 evolution and detection.

Hydrogen production experiments were performed irradiating with UV light slurries containing 1.0 g L^{-1} of TiO_2 powder of the materials and 2.0 mg L^{-1} of Pt, added as H_2PtCl_6, which is reduced to Pt^0 (by the photoelectrons produced in the semiconductor) and deposited onto TiO_2 upon irradiation. The use of a co-catalyst increases the photogenerated carrier separation improving the kinetics of H_2O reduction, which would be very slow on pristine TiO_2. The experiments were carried out at pH 3.7 using formate buffer 0.1 M (that is also the hole scavenger). The irradiation experiments were carried out in magnetically stirred, cylindrical quartz cells (3.5 cm inner diameter, 2 cm height), containing 5 mL of slurry (therefore 5 mg of material). Before irradiation the cell containing the slurry was carefully purged with nitrogen to remove oxygen from the reaction environment. The removal of oxygen is fundamental in order to avoid the competitive oxygen reduction reaction. The procedure for the experiments carried out without co-catalyst is the same but no H_2PtCl_6 was added before the irradiation.

Hydrogen and CO_2 evolution was followed sampling periodically 2.5 mL of gas from the irradiation cell and replacing it with the same volume of N_2. The gas sample was analyzed with an Agilent 490 Micro GC gas chromatograph equipped with a Molsieve 5Å column for H_2 analysis and a Poraplot U column for CO_2 quantitation. During the analysis the columns were kept at temperatures of 363 K and 313 K at a pressure of 200 kPa and 150 kPa, respectively. The carrier gases were argon and helium, respectively. The total amounts of H_2 and CO_2 produced as function of time were calculated from the concentration in the sampled gas, considering the total volume of gas in the irradiation cell and the previous samplings. The irradiation was carried out with a LED source centered at 365 nm with an irradiance of 15 W m^{-2}.

5. Photoelectrochemical Characterization

Preparation of TiO$_2$ films.

TiO$_2$ electrodes were prepared following the procedure described below:
- Preparation of 5 mL of TiO$_2$ suspension 10 g L^{-1} and sonication for 30 min;
- Deposition of a thin TiO$_2$ film on a fluorine doped tin oxide (FTO) glass using the doctor-blade technique and drying in air at room temperature;
- Dropping of the TiO$_2$ suspension over the first layer until the generation of a thick film and drying in air at room temperature. In this way all the UV irradiation was extinguished and it was possible to weight the deposited sample, but only the first layers of the film are effectively active in the photocatalytic process, decreasing the yield of the reaction;
- The illuminated area of the electrodes is 4 cm^{-2};

Apparatus and Test Conditions.

The electrochemical measurements were performed using a standard photo-electrochemical setup, composed of a computer-controlled potentiostat, AUTOLAB PGSTAT12, and a fluorescent source with λmax = 365 nm (Philips PL-S 9W BLB, integrated irradiance = 15 W m^{-2}). The electrochemical cell was a conventional three-electrode cell with a 1 mm thick fused silica window. The counter and reference electrodes were a Glassy Carbon and a Ag/AgCl/KCl (3M) electrode, respectively. Both CV and OCP measurements were carried out under a N$_2$ atmosphere (flux 200 mL min^{-1}); also the solution (0.1 M KNO$_3$ as electrolyte and 0.1 M formate buffer) was purged with N$_2$ for 30 min before each measurement in order to eliminate the residual O$_2$ present in the solution, to obtain the recombination rate of the photogenerated carriers. The Pt deposition on the TiO$_2$ films was carried out under irradiation adding the right amount of H$_2$PtCl$_6$ in order to have finally 0.2% w/w of Pt. The experiments are carried out at at pH 3.7 to reproduce the same experimental conditions adopted during photocatalytic hydrogen evolution.

Results.

Figure S7 reports the CVs of the TiO$_2$ materials at 0.1 V s^{-1}. CV is a powerful tool to probe the density of states of the semiconductor as a function of the applied potential. The Fermi level of the semiconductor can be displaced modifying the the potential at the working electrode. When the Fermi level is forced within the band gap, where the density of states is very low, the recorded current density is usually in the order of the µA cm^{-2}. Conversely, when the Fermi level is brought toward more negative values the current density increases, as the density of states does, approaching the conduction band. While a cathodic current peak was never reached, as observed in previous reports on semiconducting oxides,[6] we detected a marked anodic peak at -0.5 /-0.7 V vs Ag/AgCl depending on the material. The calcined bipyramids were characterized by larger currents, and therefore density of states, compared with the other materials. This must be taken into account when considering the CP measurements (Figure S8); in fact, the photoelectron density accumulated on bipy TiO$_2$ is significanly larger, even though the photopotentials (i.e. the difference betwwen OCP values under irradiation and in the dark) are very similar for all the specimens here considered.
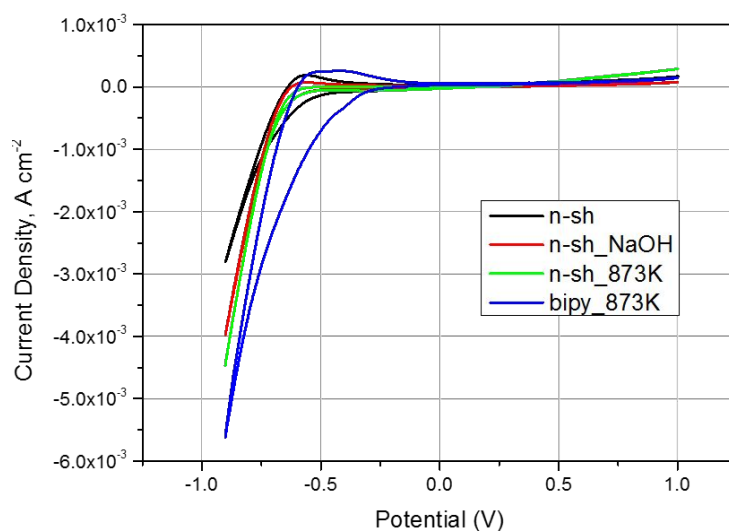
Figure S7. CV measurements carried out on the TiO$_2$ electrodes prepared starting from the studied shape controlled materials. Scan Rate 0.1 V s^{-1}

Analyzing Figure S8 we can observe that the different TiO$_2$ materials behave similarly, with more negative OCP under irradiation, and OCP relaxation toward its dark value once irradiation is interrupted (the differences in the rates of relaxation are already discussed in the main text). In the presence of Pt the electron transfer is significantly faster, and therefore the electron accumulation under irradiation is limited. This is coherent with the observation of less negative OCP under irradiation and faster OCP relaxation upon light interruption after platinization, as observed in Figure S9. In Figure S9 it is possible to see also that the photopotential is lower for all the samples due to the higher electrons depletion given by the Pt photodeposition.

From all the CPs performed we extracted the values of accumulated photoelectrons thanks to the densities of states obtained from cyclic voltammetries (using the method developed by Gomes and Monllor-Satoca in 2008)[7], following the equation:

$$n_{ph} = \frac{1}{e\,d\,A} \int_{E_{dark}}^{E_{light}} \frac{i}{s} dE$$

where e is the charge of the electron, d and A are the electrode thickness and area, respectively, i is the current recorded during the CV, s is the potential scan and E_{dark} and E_{light} are the OCP of the electrode recorded in the dark and under steady-state irradiation, respectively. From the decay of the photoelectron density in time after light discontinuation, we extracted the depletion rate constants reported in the main article (Figure 6). Gomes and Monllor-Satoca assumed photoelectron decay as a pseudo first order process with a disappearance constant k$_d$, which includes all processes (recombination and electron transfer) [7]:

$$\frac{dn_{ph}}{dt} = k_d\, n_{ph}$$

The k$_d$ value was obtained numerically differentiating the photoelectron decay with respect to time, fitting the resulting curve to the above equation.
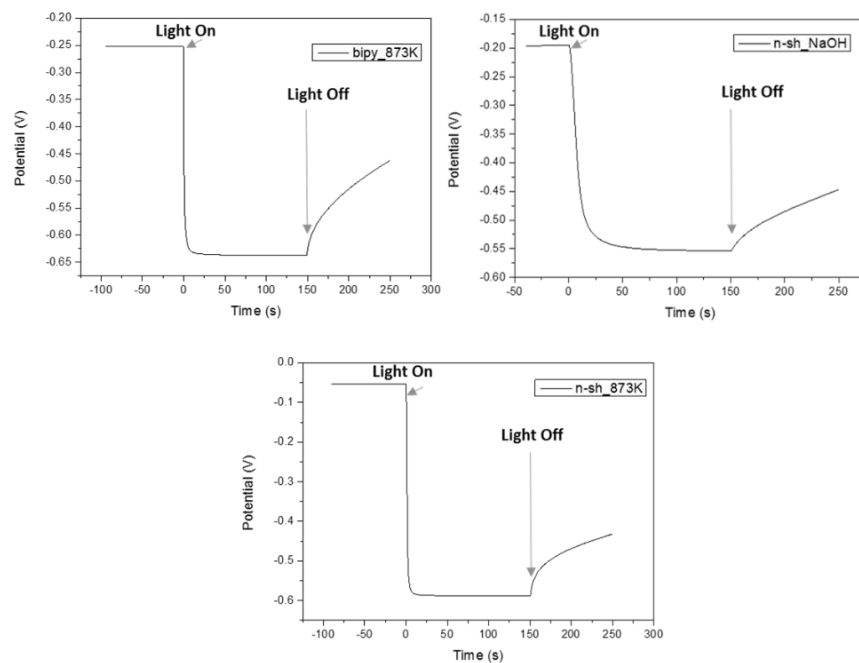
Figure S8. OCP measurements carried out on the TiO$_2$ electrodes prepared starting from the studied shape controlled materials without Pt and under N$_2$ atmosphere. pH 3.7, 0.1 M formate buffer. . The OCP of the material n-sh is in the main text (Figure 5).
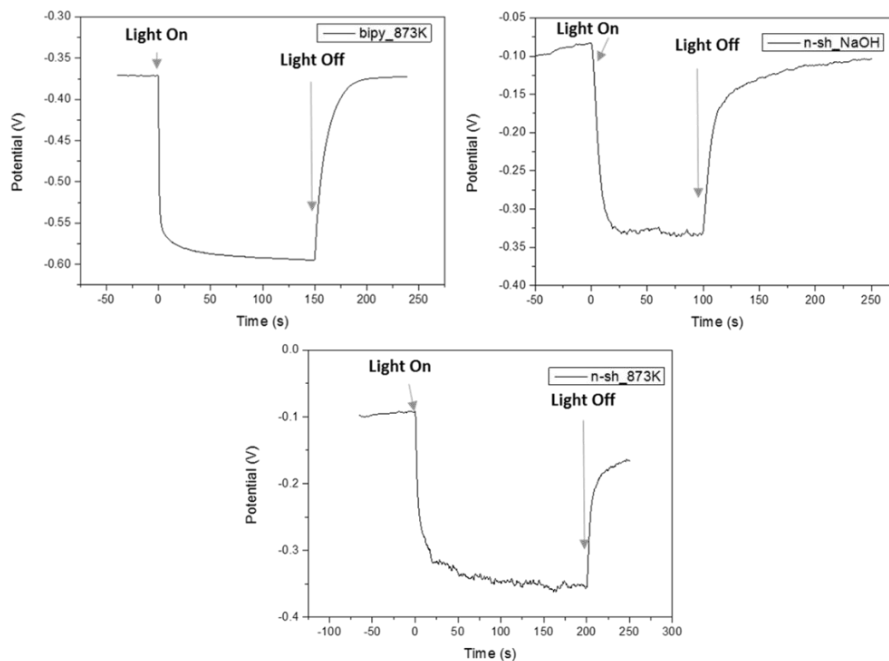

Figure S9. OCP measurements carried out on the TiO$_2$ electrodes prepared starting from the studied shape controlled materials with Pt as co-catalyst and under N$_2$ atmosphere. pH 3.7, 0.1 M formate buffer. The OCP of the material Pt/n-sh is in the main text (Figure 5).

REFERENCES

1.	Mino, L.; Pellegrino, F.; Rades, S.; Radnik, J.; Hodoroaba, V. D.; Spoto, G.; Maurino, V.; Martra, G., Beyond Shape Engineering of TiO_2 Nanoparticles: Post-Synthesis Treatment Dependence of Surface Hydration, Hydroxylation, Lewis Acidity and Photocatalytic Activity of TiO_2 Anatase Nanoparticles with Dominant {001} or {101} Facets. *Acs Applied Nano Materials* **2018,** *1*, 5355-5365.

2.	(a) Han, X.; Kuang, Q.; Jin, M.; Xie, Z.; Zheng, L., Synthesis of titania nanosheets with a high percentage of exposed (001) facets and related photocatalytic properties. *J Am Chem Soc* **2009,** *131*, 3152-3153; (b) Zhang, J.; Wang, J.; Zhao, Z.; Yu, T.; Feng, J.; Yuan, Y.; Tang, Z.; Liu, Y.; Li, Z.; Zou, Z., Reconstruction of the (001) surface of TiO_2 nanosheets induced by the fluorine-surfactant removal process under UV-irradiation for dye-sensitized solar cells. *Physical chemistry chemical physics : PCCP* **2012,** *14*, 4763-4769.

3.	Minella, M.; Faga, M. G.; Maurino, V.; Minero, C.; Pelizzetti, E.; Coluccia, S.; Martra, G., Effect of fluorination on the surface properties of titania P25 powder: an FTIR study. *Langmuir* **2010,** *26*, 2521-2527.

4.	Deiana, C.; Minella, M.; Tabacchi, G.; Maurino, V.; Fois, E.; Martra, G., Shape-controlled TiO_2 nanoparticles and TiO_2 P25 interacting with CO and H_2O_2 molecular probes: a synergic approach for surface structure recognition and physico-chemical understanding. *Phys. Chem. Chem. Phys.* **2013,** *15*, 307-315.

5.	(a) Yang, H. G.; Sun, C. H.; Qiao, S. Z.; Zou, J.; Liu, G.; Smith, S. C.; Cheng, H. M.; Lu, G. Q., Anatase TiO_2 single crystals with a large percentage of reactive facets. *Nature* **2008,** *453*, 638-641; (b) Liu, S. W.; Yu, J. G.; Jaroniec, M., Anatase TiO_2 with Dominant High-Energy {001} Facets: Synthesis, Properties, and Applications. *Chem Mater* **2011,** *23*, 4085-4093; (c) Shi, H.; Zhang, S.; Zhu, X.; Liu, Y.; Wang, T.; Jiang, T.; Zhang, G.; Duan, H., Uniform Gold-Nanoparticle-Decorated {001}-Faceted Anatase TiO_2 Nanosheets for Enhanced Solar-Light Photocatalytic Reactions. *ACS applied materials & interfaces* **2017,** *9*, 36907-36916.

6.	Fabregat-Santiago, F.; Mora-Sero, I.; Garcia-Belmonte, G.; Bisquert, J., Cyclic voltammetry studies of nanoporous semiconductors. Capacitive and reactive properties of nanocrystalline TiO_2 electrodes in aqueous electrolyte. *J. Phys. Chem. B* **2003,** *107*, 758-768.

7.	Monllor-Satoca, D.; Gomez, R., Electrochemical method for studying the kinetics of electron recombination and transfer reactions in heterogeneous photocatalysis: The effect of fluorination on TiO_2 nanoporous layers. *J Phys Chem C* **2008,** *112*, 139-147.